

Short Communication

## Synthesis of Magnesium Oxide Doped ZnO Nanostructures Using Electrochemical Deposition

Zeng Chen<sup>1</sup>, Shengjun Li<sup>1</sup>, Yafang Tian<sup>2</sup>, Shaojun Wu<sup>1</sup>, Weifeng Zhang<sup>1\*</sup>

<sup>1</sup> Key Laboratory of Photovoltaic Materials of Henan Province and School of Physics & Electronic, Kaifeng 475001, China

<sup>2</sup> Training Center of Zhengzhou Railway Vocational & Technical College, Zhengzhou 450052, China

\*E-mail: wfzhang@henu.edu.cn

Received: 4 September 2012 / Accepted: 6 October 2012 / Published: 1 November 2012

---

Zn<sub>1-x</sub>Mg<sub>x</sub>O was electrochemically deposited on fluorine doped tin oxide (FTO) conducting glass substrates. The XPS results showed that magnesium oxide was successfully doped in ZnO nanosheets. The changes of the microtopography, lattice parameters and band structure were investigated carefully. The thickness of ZnO nanosheets and the lattice parameters decreased with the addition of MgO. The transmission band-edge blue shifted and the bandgap became wider with the increasing of Mg(II) concentration in the deposition bath.

---

**Keywords:** Zn<sub>1-x</sub>Mg<sub>x</sub>O; electrodeposition; bandgap

### 1. INTRODUCTION

Semiconductor ZnO with a wide direct band gap and large excitonic binding energy at room temperature has attracted great research interest. It can be used in many areas, such as fast ultraviolet detector, light emitting diode, laser diode, gas sensors, and solar cells [1-3]. However, its bandgap is not high enough to exploit the blue region of the solar spectrum, which improves the blue response of optoelectronic devices. The bandgap of ternary Zn<sub>1-x</sub>Mg<sub>x</sub>O could be adjusted much wider than that of ZnO [4,5]. Additionally, MgO has little lattice mismatch with ZnO since the ionic radii of magnesium and zinc are relatively similar making it feasible to achieve the substitutional replacement of Zn<sup>2+</sup> with Mg<sup>2+</sup> [6]. Until now, different routes have been developed for the preparation of Zn<sub>1-x</sub>Mg<sub>x</sub>O nanostructures, such as metal organic chemical vapor deposition [6,7], pulsed laser deposition [8], molecular beam epitaxy [9], vapor phase transport [10], metal organic vapor phase epitaxy [11], sol-gel [1], RF magnetron sputtering [12], and so on.

In contrast with other techniques, the electrodeposition method shows many advantages which is usually carried out under 100 °C and could give rigid control on film thickness and composition. Various metal oxides, such as TiO<sub>2</sub>, ZnO, In<sub>2</sub>O<sub>3</sub>, and ZrO<sub>2</sub>, were successfully electrodeposited [13-16]. In addition, electrodeposition method has been used to fabricate nanostructures doped with different elements [17-19]. T. Singh et al. prepared CdO doped ZnO nanostructures using electrochemical deposition and tuned the bandgap of the deposited film from 3.32 to 3.08 eV [20]. In this article, we prepared Zn<sub>1-x</sub>Mg<sub>x</sub>O semiconductor nanostructures on FTO substrate by electrodeposition technique and studied the effects of MgO on the microtopography, lattice parameters and band structure of ZnO.

## 2. EXPERIMENTAL

The electrodeposition experiments were carried out in a simple three-electrode glass cell. The aqueous electrolyte consisted of 0.05 M Zn(NO<sub>3</sub>)<sub>2</sub> · 6H<sub>2</sub>O and 0.1 M KCl. The Mg(NO<sub>3</sub>)<sub>2</sub> · 6H<sub>2</sub>O was added to the electrolyte in a large concentration range, between 0 and 100 mM. The pH was in the range 4-6. The deposition temperature was fixed at 70 °C by an oil bath. Before electrodeposition the FTO substrates were cleaned sequentially in acetone and ethanol for 6 min each in an ultrasonic bath, followed by rinsing with flowing DI water. Afterward, these substrates were immersed in HNO<sub>3</sub> (45%) for 2 min and finally rinsed in DI water for 5 min in an ultrasonic bath [21]. The working electrode was FTO glass substrates (10 mm × 10 mm). The reference electrode was Ag/AgCl electrode with saturation potassium chloride aqueous solution and the counter electrode was Pt metal sheet. Electrochemical deposition experiments were carried out at constant current density of 3 mA cm<sup>-2</sup> for 5 min with CHI660C electrochemical workstation (Shanghai Chen- hua Instrument Co, China). The deposited samples were cleaned with DI water, dried at room temperature and annealed at 400 °C for 30 min in the air.

The crystalline phase of the samples was characterized by DX-2700 X-ray diffractometer (XRD) with a monochromatized Cu K $\alpha$  irradiation ( $\lambda = 0.154145$  nm) and morphologies were determined using a HitachiS-4300F field emission scanning electron microscope (SEM). X-ray photoelectron spectroscopy (XPS, AXIS ULTRA) was used to assess the chemical state and surface composition of the deposits. The transmission spectrum was measured by a UV-vis-NIR photospectrometer (Varian Cary 5000).

## 3. RESULTS AND DISCUSSION

SEM images of pure ZnO and Zn<sub>1-x</sub>Mg<sub>x</sub>O nanostructures synthesized by electrodeposition approach are presented in Fig. 1. Fig. 1(a) shows the SEM image of pure ZnO prepared in a solution of 0.05 M Zn(NO<sub>3</sub>)<sub>2</sub> and 0.1 M KCl with constant current density of 3 mA cm<sup>-2</sup> at 70 °C. Fig. 1(b) shows the SEM image of Zn<sub>1-x</sub>Mg<sub>x</sub>O nanosheets prepared in a solution of 0.1 M Mg(NO<sub>3</sub>)<sub>2</sub> + 0.05 M Zn(NO<sub>3</sub>)<sub>2</sub> + 0.1 M KCl with constant current density of 3 mA cm<sup>-2</sup> at 70 °C. We have observed an decrease of the thickness of nanosheet with the addition of Mg(II) in the deposition bath.

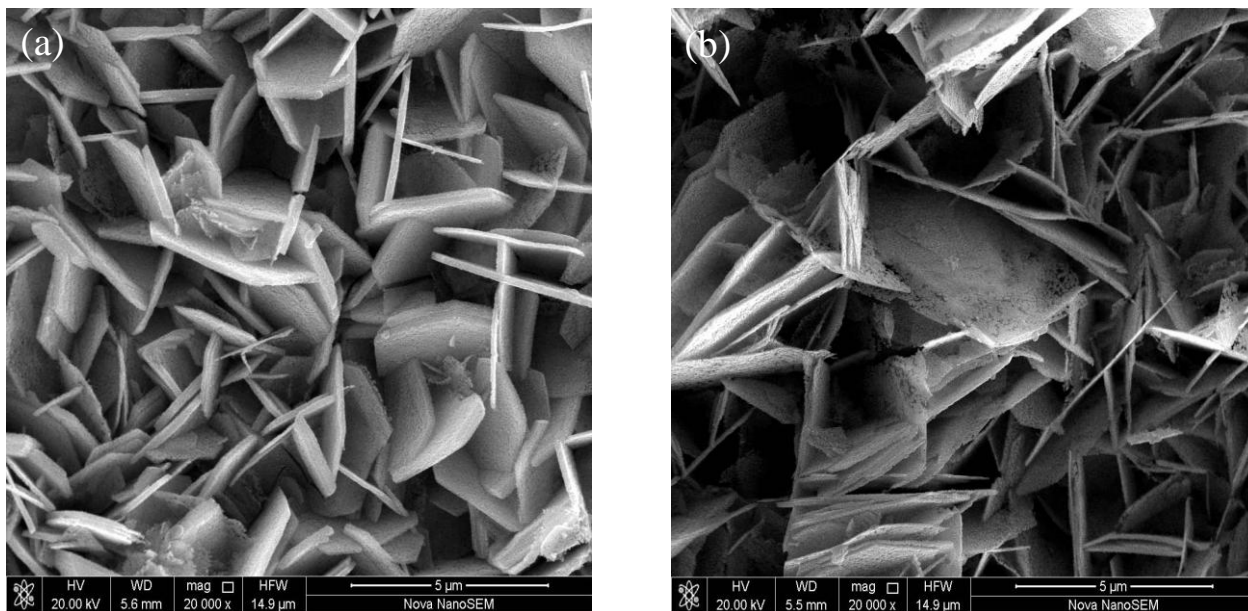
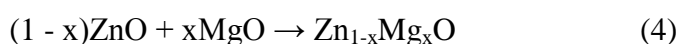
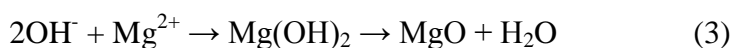
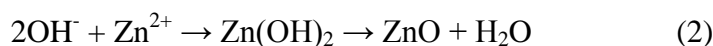


**Figure 1.** SEM images of pure ZnO and Zn<sub>1-x</sub>Mg<sub>x</sub>O nanosheets prepared in solution of (a) 0.05 M Zn(NO<sub>3</sub>)<sub>2</sub> + 0.1 M KCl and (b) 0.1 M Mg(NO<sub>3</sub>)<sub>2</sub> + 0.05 M Zn(NO<sub>3</sub>)<sub>2</sub> + 0.1 M KCl with constant current density of 3 mA cm<sup>-2</sup> at 70 °C.

To clarify the structural properties of ZnO and Zn<sub>1-x</sub>Mg<sub>x</sub>O films, X-ray diffraction experiments have been carried out. Fig. 2 shows the XRD patterns of pure ZnO and Mg-alloyed ZnO films prepared with different Mg<sup>2+</sup> concentrations (5 mmol/L, 30 mmol/L and 100 mmol/L). XRD studies of the crystal structure indicate only peaks of wurtzite-structured ZnO (hexagonal phase, space group *P63mc*) (JCPDS database card No. 36-1451). The relational Mg(OH)<sub>2</sub> or MgO crystalline forms are not detected in the XRD pattern, which revealed that the incorporation of magnesium could not affect the wurtzite phase of ZnO. The growth mechanism can be explained by the following reaction:



During the electrodeposition process, the NO<sub>3</sub><sup>-</sup> was electroreduced on the cathode, and the hydroxyl ions (OH<sup>-</sup>) were produced according to Eq. (1). Then the hydroxyl group emerged at the surface of cathodic electrode and reacted with metal ions Zn<sup>2+</sup> and Mg<sup>2+</sup> coming from the solution to form metal oxide according to Eq. (2) and Eq.(3), respectively. Finally, ZnO and MgO mixed at atomic levels and formed Zn<sub>1-x</sub>Mg<sub>x</sub>O.

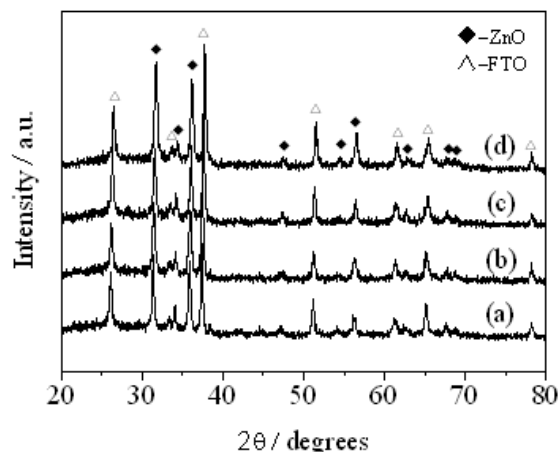


**Figure 2.** XRD patterns of the ZnO and  $\text{Zn}_{1-x}\text{Mg}_x\text{O}$  films obtained from electrodeposition baths containing 0.05 mol/L  $\text{Zn}(\text{NO}_3)_2$  and different  $\text{Mg}(\text{NO}_3)_2$  concentration: 0mmol/L (a), 5mmol/L (b), 30 mmol/L (c), and 100 mmol/L (d), respectively.

Furthermore, we observed a shift of the main Bragg peak (101) to larger angle from Fig. 2 which indicated the changes in the lattice parameters due to strain in the host on incorporation of the dopant ions into the basic unit cell. For the bulk ZnO, the reported values of the lattice constants are  $a = b = 3.250 \text{ \AA}$ ,  $c = 5.207 \text{ \AA}$  [JCPDS Card No. 36-1451]. From the position of the peak, lattice constants with and without Mg doping can be calculated. The lattice constants have been calculated for various concentrations of Mg in the hexagonal crystal lattice of ZnO and the results are presented in Table 1. It shows that the lattice parameters decrease with increasing  $\text{Mg}^{2+}$  content in the deposition bath. This is consistent with the smaller magnesium ionic radius ( $0.57 \text{ \AA}$ ) compared to the zinc ionic radius ( $0.60 \text{ \AA}$ ) [22]. The lattice parameter of  $\text{Zn}_{1-x}\text{Mg}_x\text{O}$  thin films obeyed Vegard's law, indicated solid solution might exist. The lattice stress  $\sigma_f$  (shown in Table 1) of the nanostructures has been calculated using the expression.

$$\sigma_f = 2.33 \times 10^{11} \times \frac{c_b - c_f}{c_b} \quad (5)$$

Where  $c_b$  and  $c_f$  are the lattice constant  $c$  of the bulk ZnO and grown nanostructure films, respectively. The positive sign of estimated stress for the doped ZnO indicates that the crystallites are under a state of tensile stress.

**Table 1.** Computed lattice parameters and band gap of pure ZnO and  $\text{Zn}_{1-x}\text{Mg}_x\text{O}$  samples annealed at  $400 \text{ }^\circ\text{C}$ .

Sample	$\text{Mg}^{2+}$ , 0 mM	$\text{Mg}^{2+}$ , 5 mM	$\text{Mg}^{2+}$ , 30 mM	$\text{Mg}^{2+}$ , 100 mM
$a$ ( $\text{\AA}$ )	3.289	3.279	3.269	3.256
$c$ ( $\text{\AA}$ )	5.257	5.245	5.237	5.212
$\sigma_f$	0	$0.532 \times 10^9$	$0.886 \times 10^9$	$1.994 \times 10^9$
Band gap (eV)	3.203	3.228	3.243	3.280

The film surface composition was analyzed by the XPS technique. A survey scan of XPS spectra of  $Zn_{1-x}Mg_xO$  films with the sheet nanostructures grown from 5 mmol/L  $Mg(NO_3)_2$  aqueous solution containing 0.05 M  $Zn(NO_3)_2$  were shown in Fig. 3(a). Fig. 3(b) and (c) show the high-resolution scans of Zn 2p and O 1s, respectively. The peaks located at 1021 and 1044 eV corresponded to Zn 2p<sub>3/2</sub> and Zn 2p<sub>1/2</sub>, respectively. The peak located at 530 eV should be corresponded to the electronic state of O 1s. The Mg 2s binding energy spectra are shown in Fig. 3(d). The high-binding and low-binding energy components at 88 and 91 eV, respectively, were from magnesium oxide and zinc oxide, which demonstrates the existence of  $Mg^{2+}$  in the deposited coating[22].

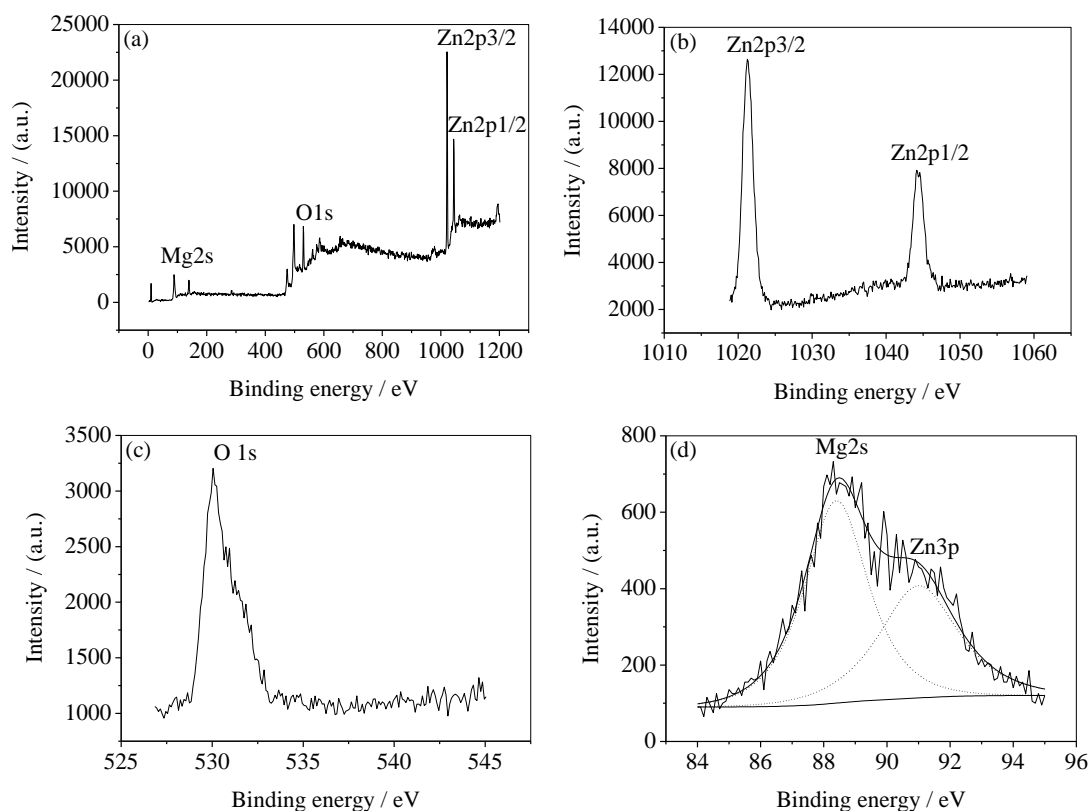


**Figure 3.** XPS spectra of  $Zn_{1-x}Mg_xO$  composite films obtained from electrodeposition baths containing 0.05 mol/L  $Zn(NO_3)_2$  and 5 mmol  $Mg(NO_3)_2$ : Survey scan (a), and high-resolution scans of Zn region(b), O region(c), Mg region(d).

The optical transmittance spectra of the  $Zn_{1-x}Mg_xO$  thin films were recorded in the wavelength range of 300-800 nm at room temperature. The optical absorption data was analyzed using the following classical relation (Eq. 6) of optical absorption in semiconductor near band edge [23,24].

$$\alpha = \frac{A(h\nu - E_g)^n}{h\nu} \quad (6)$$

Where  $A$  is a constant,  $E_g$  is the energy gap and  $n = 1/2$  for direct transition, and  $h\nu$  is the energy of incident photon. Fig. 4 shows the  $(\alpha h\nu)^2$  versus  $(h\nu)$  curves of  $Zn_{1-x}Mg_xO$  thin films prepared

with different  $\text{Mg}^{2+}$  concentrations in the electrolyte (0 mmol/L, 5 mmol/L, 30 mmol/L and 100 mmol/L). The absorption edge was found to shift toward the shorter wavelength side as more and more magnesium was incorporated. The band-edge blue shifted is due to a bandgap wider of the material with increasing of  $\text{Mg}^{2+}$  concentrations in the deposition bath. The bandgap was approximated by plotting  $(\alpha h\nu)^2$  versus  $(h\nu)$  and extrapolating the linear part of the curve to the  $x$ -axis. The obtained values of bandgap energy were shown in Table 1. These values of bandgap energy varied from 3.20 eV to 3.28 eV with the increasing of  $\text{Mg}(\text{II})$  concentration in the deposition bath.

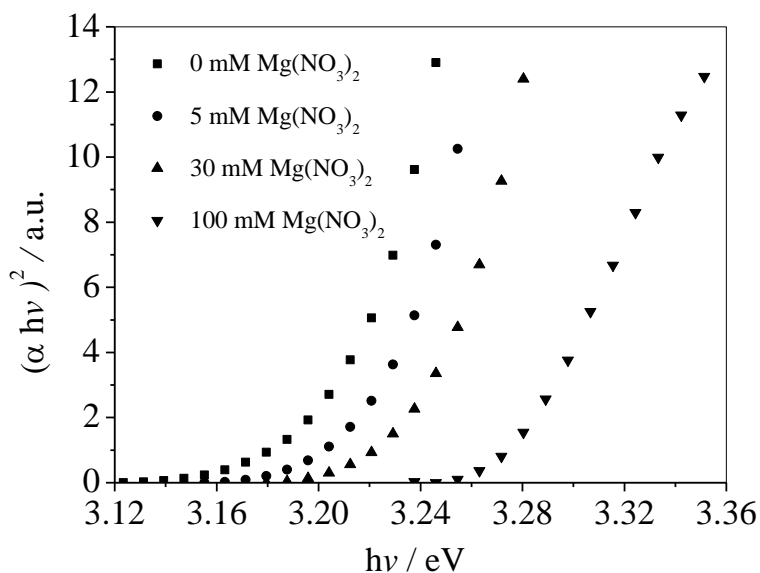


**Figure 4.** Optical absorption spectra of the  $\text{ZnO}$  and  $\text{Zn}_{1-x}\text{Mg}_x\text{O}$  composite films obtained from electrodeposition baths containing 0.05 mol/L  $\text{Zn}(\text{NO}_3)_2$  and different  $\text{Mg}(\text{NO}_3)_2$  concentration: 0mmol/L (a), 5mmol/L (b), 30 mmol/L (c), and 100 mmol/L (d), respectively.

#### 4. CONCLUSION

In summary,  $\text{Zn}_{1-x}\text{Mg}_x\text{O}$  thin films were fabricated on FTO substrate by electrodeposition method. The effects of the magnesium content on the structural and optical properties were studied. XRD analysis showed that the  $\text{Zn}_{1-x}\text{Mg}_x\text{O}$  thin film possessed wurtzite structure. Structural changes have also been observed by XRD studies which have been explained by the partial replacement of Zn atoms by Mg atoms in the lattice structure which was confirmed by a computational study. The transmission band-edge blue shifted and the bandgap became wider with the increasing of  $\text{Mg}(\text{II})$  concentration in the deposition bath. The band gap energy varied from 3.20 eV – 3.28 eV.

#### ACKNOWLEDGEMENTS

This work was supported by the Program for Innovative Research Team in Science and Technology in University of Henan Province (IRTSTHN) (Grant No.2012IRTSTHN004), the Basic and Frontier Technology Research Programs of the Department of Science & Technology of Henan Province (No. 112300410004 and No. 122300410107) and the Research Fund of Henan University (No. 2010ZRZD07).

## References

1. A. Singh, D. Kumar, P. K. Khanna, A. Kumar, M. Kumar, M. Kumar, *Thin Solid Films*, 519 (2011) 5826,.
2. O. Isabella, F. Moll, J. Krc, M. Zeman, *Phys. Status Solidi A*, 207 (2010) 642,.
3. F. Xu, M. Dai, Y. N. Lu, L. T. Sun, *J. Phys. Chem. C*, 114 (2010) 2776,.
4. P. Prathap, N. Revathi, A. Suryanarayana Reddy, Y. P. Venkata Subbaiah, K. T. Ramakrishna Reddy, *Thin Solid Films*, 519 (2011) 7592.
5. J. Li, J. Huang, W. Song, R. Tan, Y. Yang, X. Li, *J. Mater. Sci. Mater. Electron.* 21 (2010) 529.
6. A. M. Torres-Huerta, M. A. Domínguez-Crespo, S. B. Brachetti-Sibaja, J. Arenas-Alatorre, A. Rodríguez-Pulido, *Thin Solid Films* 519 (2011) 6044.
7. L. L. Yang, Q. X. Zhao, G. Z. Xing, D. D. Wang, T. Wu, M. Willander, I. Ivanov, J. H. Yang, *Applied Surface Science*, 257 (2011) 8629.
8. W. Yang, S. S. Hullavarad, B. Nagaraj, I. Takeuchi, R. P. Sharma, T. Venkatesan, R.D. Vispute, *Applied Physics Letters*, 82 (2003) 3424.
9. K. Ogata, K. Koike, T. Tanite, T. Komuro, F. Yan, S. Sasa, M. Inoue, M. Yano, *Jouranal of Crystal Growth*, 251 (2003) 623.
10. H. C. Hsu, C. Y. Wu, H. M. Cheng, W. F. Hsieh, *Appl. Phys. Lett.*, 89 (2006) 013101.
11. R. Kling, C. Kirchner, T. Gruber, F. Reuss, A. Waag, *Nanotechnology* 15 (2004) 1043.
12. T. Minemoto, T. Negami, S. Nishiwak, *Thin Solid Films*, 372 (2000) 173.
13. J. B. Zhang, L. Sun, K. Ichinose, K. Funabiki, T. Yoshida, *Phys Chem Chem Phys*, 2010; 12: 10494.
14. K. Wessels, M. Wark, T. Oekermann, *Electrochim. Acta*, 55 (2010) 6352.
15. B. Ferrari, R. Moreno, *J. Electrochem. Soc.*, 147 (2000) 2987.
16. R. Sharma, R. S. Mane, S. K. Min, S. H. Han, *J. Allows Compd.*, 479 (2009) 840.
17. F. Fang, A. M. C. Ng, X. Y. Chen, A. B. Djurišić, Y. C. Zhong, K. S. Wong, P. W. K. Fong, H. F. Lui, C. Surya, W. K. Chan, *Mater. Chem. Phys.*, 125 (2011) 813.
18. G. R. Li, C. R. Dawa, X. H. Lu, X. L. Yu, Y. X. Tong, *Langmuir* ,25 (2009) 2378.
19. S. Q. Wei, Y. Y. Chen, Y. Y. Ma, Z. C. Shao. *J. Mol. Catal. A* ,331 (2010) 112.
20. Triok Singh, D. K. Pandya, R. Singh, *J. Alloys Comod.*, 509 (2011) 5095.
21. O. Lupan, T. Pauporté, T. L. Bahers, I. Ciofini, B. Viana, *J. Phys. Chem. C*, 115 (2011) 14548.
22. H. Ishizaki, N. Yamada, *Electrochem. Sol. State Lett.*, 9 (2006) C178.
23. K. Ogata, K. Koikeb, T. Taniteb, T. Komuro, F. Yan, S. Sasa, M. Inoue, M. Yano, *J. Crystal Growth*, 25 (2003) 623
24. F. B. Micheletti, P. Mark, *Appl. Phys. Lett.*, 10 (1967) 136